Blind Symbol Timing and CFO Estimation for OFDM/OQAM Systems

Davide Mattera and Mario Tanda

***Abstract*—The paper deals with the problem of blind synchronization for OFDM/OQAM systems. Specifically, by exploiting the approximate conjugate-symmetry property of the beginning of a burst of OFDM/OQAM symbols, due to the presence of the time offset, a new procedure for blind symbol timing and CFO estimation is proposed. The performance of the derived blind estimators is analyzed by computer simulations; the results show that the proposed methods may provide acceptable performance for reasonable values of the signal-to-noise ratio.**

***Index Terms*—OFDM/OQAM, multicarrier systems, prototype filter, FBMC, synchronization, symbol timing, CFO.**

I. Introduction

In the last years, the interest for filter-bank multicarrier (FBMC) systems is increased, since they provide high spectral containment. Therefore, they have been taken into account for high-data-rate transmissions over both wired and wireless frequency-selective channels. One of the most famous multicarrier modulation techniques is orthogonal frequency division multiplexing (OFDM), other known types of FBMC systems are filtered multitone systems [1], [2] and OFDM based on offset QAM modulation (OQAM) [3], [4], [5], [6].

The FBMC approach complements the FFT with a set of digital filters called polyphase network (PPN) while the OFDM approach inserts the cyclic prefix (CP) after the FFT. Unlike OFDM, OFDM/OQAM systems do not require the presence of a CP in order to combat the effects of frequency selective channels. The absence of the CP implies on the one hand the maximum spectral efficiency and, on the other hand, an increased computational complexity. However, since the subchannel filters are obtained by complex modulation of a single filter, efficient polyphase implementations is often considered [7]. Fundamental differences between OFDM and OFDM/OQAM systems concern the adoption (in the OFDM/OQAM case) of pulse shaping filters very well localized in time and frequency [8], [9] and memory effects between useful symbols and transmitted signal due to the PPN.

OFDM/OQAM systems, as all multicarrier systems, are more sensitive to synchronization errors than single-carrier systems. For this reason, it is very important to derive efficient synchronization schemes. In the last years several studies have been focused on blind and data-aided carrier frequency-offset (CFO) and symbol timing (ST) synchronization for OFDM/OQAM systems. New proposals aim at simplifying the structure of the preamble in order to be able to use it for synchronization and equalization purposes. In [10] a synchronization scheme for preamble-based ST and CFO estimation with robust acquisition properties in dispersive channels has been developed. In [11] a new preamble structure has been proposed with useful properties that simplify the use of a one-tap equalizer. The characteristics of the preamble derive from the need to simplify the procedures for channel estimation. The resulting synchronization algorithms become dependent on the particular preamble, whose utilization is obviously conditioned by the availability of a proper synchronization method. Therefore, a general contribution to the development of synchronization algorithms requires the capability to operate without any specific knowledge about the structure of the preamble. Obviously, this not only represents a preamble-independent contribution to the synchronization task, which allows a standard definition of the preamble structure unconstrained by the requirements of the synchronization algorithms, but also paves the way to an increase of the spectral efficiency to be achieved by avoiding the preamble.

The blind estimation algorithm proposed in [12] is based on the exploitation of the second-order cyclostationarity of the transmitted OFDM/OQAM signal; the convergence of such a method is particularly slow (too many symbol periods have to be processed) so that it is not useful in practice, unless severe signal-to-noise ratios are considered. Moreover, it is limited to the case where CFO is present but it is not dedicated to the joint CFO and timing offset estimation. However, [13] considers the case where both the offsets are jointly estimated by exploiting the cyclostationarity properties. In [14] an algorithm for blind CFO estimation is also proposed according to an approximate (for a large number of subcarriers) maximum-likelihood approach and it is shown its superior performance in comparison with the cyclostationarity-based methods. Moreover, in [15] a maximum likelihood method for blind CFO estimation suited for scenarios of low signal-to-noise ratio is proposed. However, the weak point of both proposed methods lies in their computational complexity.

In this paper, we analyze the conjugate-symmetry property that approximately holds in the beginning of a burst of OFDM/OQAM symbols. Using such an approximate property, a blind method for joint ST and CFO estimation is proposed. Although the proposed method is derived with reference to an AWGN channel, it is analyzed by computer simulation with reference to standard multipath channels; the numerical

Manuscript received February 29, 2012; accepted October 9, 2012. The associate editor coordinating the review of this paper and approving it for publication was S. Sfar.

The authors are with the 'Dipartimento di Ingegneria Biomedica, Elettronica e delle Telecomunicazioni', Università degli Studi di Napoli Federico II, Via Claudio, 21, I-80125 Napoli, Italy (e-mail: {mattera, tanda}@unina.it).

This work was partially supported by the European Commission under Project PHYDYAS (FP7-ICT-2007-1-211887).

Digital Object Identifier 10.1109/TWC.2012.121112.120296

results show that the proposed method can represent a useful contribution to the blind timing synchronization when the OFDM/OQAM system operates over a multipath channel. Moreover, the same analysis shows that the proposed method provides a useful contribution to the coarse CFO compensation only for adequate signal-to-noise ratios. Preliminary results about the analysis of the approximate conjugate-symmetry property in the beginning of a burst of OFDM/OQAM symbols and its exploitation for ST and CFO estimation are reported in [16].

The paper is organized as follows. In Section II the OFDM/OQAM system model is delineated. In Section III the conjugate symmetry property (CSP) and the methods to detect it are recalled. In Section IV it is derived the proposed blind ST estimator exploiting the approximate CSP. In Section V the proposed blind CFO estimation method is described. In Section VI the performance analysis of the proposed blind estimators, carried out by computer simulations, is presented and discussed. Finally, conclusions are drawn in Section VII.

Notation: $j \triangleq \sqrt{-1}$, superscript $(\cdot)^*$ denotes the complex conjugation, $\Re[\cdot]$ the real part, $\Im[\cdot]$ the imaginary part, $\delta(\cdot)$ the Kronecker delta, $|\cdot|$ the absolute value and $\angle[\cdot]$ the argument of a complex number in $[-\pi, \pi)$. Moreover, lowercase boldface letters denote column vectors, $\cdot$ the scalar product, $\|\mathbf{x}\| \triangleq \sqrt{\mathbf{x}\cdot\mathbf{x}}$ the norm, $\times$ the component-wise product between two vectors and, finally, $\mathbf{0}$ and $\mathbf{1}$ denote, respectively, the null vector and the vector whose entries are all ones.

II. System Model

Let us consider an OFDM/OQAM system with an even number M of subcarriers. The received signal when the information-bearing signal $s(t)$ presents a timing offset τ, a CFO normalized to subcarrier spacing $\epsilon = \Delta f T$ and a carrier phase offset ϕ, can be written as

$$r(t) = e^{j\frac{2\pi}{T}\epsilon t} e^{j\phi} s(t-\tau) + n(t) \tag{1}$$

where $n(t)$ is a zero-mean complex-valued white Gaussian noise process with independent real and imaginary part, each with two-sided power spectral density N_0. The signal $s(t)$ is equal to

$$s(t) = s^{\mathrm{R}}(t) + j s^{\mathrm{I}}(t - T/2) \tag{2}$$

with

$$s^{\mathrm{R}}(t) = \sum_{n=0}^{N_{\mathrm{b}}+N_{\mathrm{s}}-1} \sum_{m\in\mathcal{A}} a^{\mathrm{R}}_{n,m} e^{jm\left(\frac{2\pi}{T}t+\frac{\pi}{2}\right)} g(t-nT) \tag{3}$$

$$s^{\mathrm{I}}(t) = \sum_{n=0}^{N_{\mathrm{b}}+N_{\mathrm{s}}-1} \sum_{m\in\mathcal{A}} a^{\mathrm{I}}_{n,m} e^{jm\left(\frac{2\pi}{T}t+\frac{\pi}{2}\right)} g\left(t-nT\right) \tag{4}$$

where T is the OFDM/OQAM symbol interval, $\mathcal{A} \subset \{0,\ldots,M-1\}$ is the set of size M_u of active subcarriers, the sequences $a^{\mathrm{R}}_{n,m}$ and $a^{\mathrm{I}}_{n,m}$ indicate the real and imaginary part of the complex data symbols transmitted on the mth subcarrier during the nth OFDM/OQAM symbol, N_{b} is the number of training symbols, N_{s} is the number of payload symbols, while $g(t)$ is the prototype filter. Note that we assume that both the training symbols and the payload symbols are unknown.

The discrete-time low-pass version of the transmitted signal is given by

$$\begin{aligned} s[i] &\triangleq s(t)|_{t=iT_{\mathrm{s}}} \\ &= s^{\mathrm{R}}(iT_{\mathrm{s}}) + j s^{\mathrm{I}}((i-M/2)T_{\mathrm{s}}) \end{aligned} \tag{5}$$

where $T_{\mathrm{s}} \triangleq T/M$ is the sampling interval. Let us first consider the derivation of an efficient generation procedure for the signal $s^{\mathrm{R}}(t)$. An analogous derivation can be straightforwardly obtained for the signal $s^{\mathrm{I}}(t)$.

Since the continuous-time signal is generated by D/A conversion, we consider the generation of its discrete-time samples

$$\begin{aligned} s^{\mathrm{R}}[i] &\triangleq s^{\mathrm{R}}(iT_{\mathrm{s}}) \\ &= \sum_{n=0}^{N_{\mathrm{b}}+N_{\mathrm{s}}-1} \sum_{m\in\mathcal{A}} a^{\mathrm{R}}_{n,m} e^{jm\left(\frac{2\pi}{T}iT_{\mathrm{s}}+\frac{\pi}{2}\right)} g(iT_{\mathrm{s}} - nMT_{\mathrm{s}}) \\ &= \sum_{n=0}^{N_{\mathrm{b}}+N_{\mathrm{s}}-1} \sum_{m\in\mathcal{A}} a^{\mathrm{R}}_{n,m} e^{jm\left(\frac{2\pi}{M}i+\frac{\pi}{2}\right)} g((i-nM)T_{\mathrm{s}}) \end{aligned} \tag{6}$$

The generation of the sequence $s^{\mathrm{R}}[i]$ is equivalent to the generation of the sequence of vectors $\mathbf{d}^{(\mathrm{R})}_n$ defined as the $M \times 1$ vector whose mth component, say $d^{(\mathrm{R})}_{n,m}$, is equal to $s^{\mathrm{R}}[nM+m]$ for $m \in \{0,1,\ldots,M-1\}$. Such a component can be written as

$$\begin{aligned} d^{(\mathrm{R})}_{n,m} &\triangleq s^{\mathrm{R}}[nM+m] \qquad\qquad m \in \{0,1,\ldots,M-1\} \\ &= \sum_{n'=0}^{N_{\mathrm{b}}+N_{\mathrm{s}}-1} \sum_{m'\in\mathcal{A}} a^{\mathrm{R}}_{n',m'} e^{jm'\left(\frac{2\pi}{M}(nM+m)+\frac{\pi}{2}\right)} \\ &\times\ g((nM+m-n'M)T_{\mathrm{s}}) \\ &= \sum_{n'=0}^{N_{\mathrm{b}}+N_{\mathrm{s}}-1} \sum_{m'\in\mathcal{A}} (j^{m'} a^{\mathrm{R}}_{n',m'}) e^{jm'\frac{2\pi}{M}m} \\ &\times\ g((m+(n-n')M)T_{\mathrm{s}}) \end{aligned} \tag{7}$$

$$= \sum_{n'=0}^{N_{\mathrm{b}}+N_{\mathrm{s}}-1} b^{(\mathrm{R})}_{n',m}\ g((m+(n-n')M)T_{\mathrm{s}}) \tag{8}$$

where we have denoted with $b^{(\mathrm{R})}_{n,m}$ just the quantity

$$\sum_{m'\in\mathcal{A}} (j^{m'} a^{\mathrm{R}}_{n,m'}) e^{jm'\frac{2\pi}{M}m} \qquad m \in \{0,1,\ldots,M-1\} \tag{9}$$

which is the IDFT of the sequence $j^m a^{\mathrm{R}}_{n,m}$ with respect to the index m. If we define the vector $\mathbf{b}^{(\mathrm{R})}_n$ as the $M \times 1$ vector whose mth component (for $m \in \{0,1,\ldots,M-1\}$) is $b^{(\mathrm{R})}_{n,m}$ in (9), we can synthetically write

$$\mathbf{b}^{(\mathrm{R})}_n = \mathrm{IDFT}\ [\mathbf{w} \times \mathbf{a}^{(\mathrm{R})}_n] \tag{10}$$

where $\mathrm{IDFT}[\cdot]$ denotes the IDFT operator on the input vector and, for $m \in \mathcal{A}$, the mth component w_m of the M-vector $\mathbf{w}$ is $w_m = j^m$ and the mth component of the vector $\mathbf{a}^{(\mathrm{R})}_n$ is the symbol $a^{\mathrm{R}}_{n,m}$ in (3) while, for $m \notin \mathcal{A}$, $w_m = 0$ and the components of $\mathbf{a}^{(\mathrm{R})}_n$ are irrelevant. Note that (10) is only defined for $n \in \{0,1,\ldots,N_{\mathrm{b}}+N_{\mathrm{s}}-1\}$ but we can straightforwardly extend it to any n provided that we assume

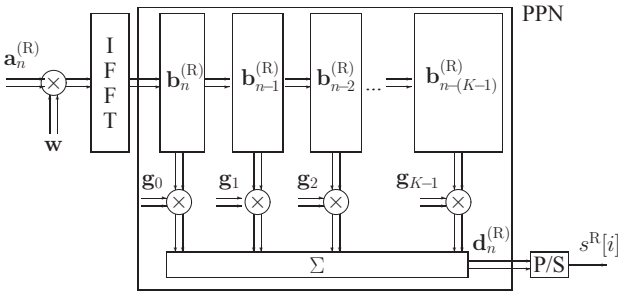

Fig. 1. Structure for generating the term $s^{\mathrm{R}}[i]$ in (6).

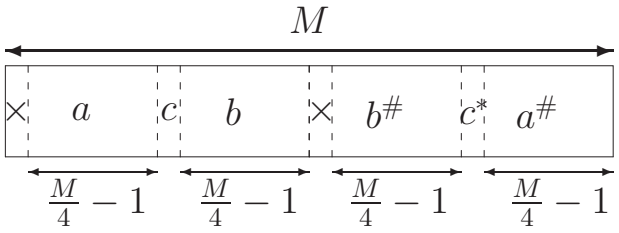

Fig. 2. Structure of the OFDM symbol for $\mathbf{a}_n^{(\mathrm{I})}=\mathbf{0}$ [17] where a and b denote the positions where the CSP holds with respect to the positions $a^{\#}$ and $b^{\#}$, respectively, c denotes a single position where the CSP holds with respect to the position c^* but it is not used, and, finally, $\times$ denotes positions where no CSP holds.

that $\mathbf{a}_n^{(\mathrm{R})}\equiv\mathbf{b}_n^{(\mathrm{R})}\equiv\mathbf{0}$ when $n\notin\{0,1,\ldots,N_{\mathrm{b}}+N_{\mathrm{s}}-1\}$. We can synthetically write the relation (8) as

$$\mathbf{d}_n^{(\mathrm{R})}=\sum_{n'=0}^{N_{\mathrm{b}}+N_{\mathrm{s}}-1}\mathbf{b}_{n'}^{(\mathrm{R})}\times\mathbf{g}_{n-n'} \tag{11}$$

where the vector $\mathbf{g}_n$ is defined so that its mth component $g_{n,m}$ is

$$g_{n,m}\triangleq g((m+nM)T_{\mathrm{s}}) \qquad m\in\{0,1,\ldots,M-1\}. \tag{12}$$

Since the prototype filter $g(t)$ can be nonnull only in the interval $[0,KT)$, it follows that the vector $\mathbf{g}_n$ can be nonnull only for $n\in\{0,1,\ldots,K-1\}$, where K is the overlap parameter, that is, the ratio between the length of the prototype filter $g(t)$ and the multicarrier symbol interval T. Consequently, (11) can be rewritten as

$$\mathbf{d}_n^{(\mathrm{R})}=\mathbf{g}_0\times\mathbf{b}_n^{(\mathrm{R})}+\mathbf{g}_1\times\mathbf{b}_{n-1}^{(\mathrm{R})}+\ldots+\mathbf{g}_{K-1}\times\mathbf{b}_{n-(K-1)}^{(\mathrm{R})}. \tag{13}$$

A block diagram of the structure for the efficient generation of the term $s^{\mathrm{R}}[i]$ in (6) is reported in Fig. 1. Analogously, the generation of the sequence $s^{(\mathrm{I})}[i]$ in (5) is equivalent to the generation of the sequence of vectors $\mathbf{d}_n^{(\mathrm{I})}$ defined as the output of the PPN:

$$\mathbf{d}_n^{(\mathrm{I})}=\mathbf{g}_0\times\mathbf{b}_n^{(\mathrm{I})}+\mathbf{g}_1\times\mathbf{b}_{n-1}^{(\mathrm{I})}+\ldots+\mathbf{g}_{K-1}\times\mathbf{b}_{n-(K-1)}^{(\mathrm{I})} \tag{14}$$

with

$$\mathbf{b}_n^{(\mathrm{I})}\triangleq\mathrm{IDFT}[\mathbf{a}_n^{(\mathrm{I})}\times\mathbf{w}] \tag{15}$$

where the mth component ($m\in\mathcal{A}$) of the vector $\mathbf{a}_n^{(\mathrm{I})}$ is the symbol $a_{n,m}^{\mathrm{I}}$ in (4).

III. The Exact Conjugate-Symmetry Property in OFDM

In OFDM systems the vector $\mathbf{w}$ in (15) has unit components, the PPN and the offset of $M/2$ samples are not present, i.e., the vector $\mathbf{d}_n^{(\mathrm{R})}+j\mathbf{d}_n^{(\mathrm{I})}$ is defined as $\mathrm{IDFT}[\mathbf{a}_n^{(\mathrm{R})}+j\mathbf{a}_n^{(\mathrm{I})}]$ and it is transmitted after cyclic-prefix extension. Therefore, if $\mathbf{a}_n^{(\mathrm{I})}=\mathbf{0}$, the vector $\mathbf{d}_n^{(\mathrm{R})}+j\mathbf{d}_n^{(\mathrm{I})}=\mathbf{d}_n^{(\mathrm{R})}$ possesses the well-known CSP, as synthetically depicted in Fig. 2.

In the transmitted multicarrier symbol, the cyclic prefix is followed by M samples that possess the CSP: if such M samples are collected in the vector $[u_0\ \mathbf{u}_1\ u_{M/2}\ \mathbf{u}_2]$ (where the length of both vectors $\mathbf{u}_1$ and $\mathbf{u}_2$ is $M/2-1$), then $\mathbf{u}_1=\mathbf{u}_2^{\#}$ where $\mathbf{u}_2^{\#}$ denotes the flipped and conjugate version of $\mathbf{u}_2$ (i.e., the mth entry of $\mathbf{u}_1$, denoted as $u_{1,m}$, is equal to $u_{2,M/2-2-m}^*$ for $m=0,1,\ldots,M/2-2$). In the signal received on a flat channel in the absence of noise and frequency offset, each cyclic prefix is followed by M samples that possess the CSP: if such M samples are collected in the vector $[u_0e^{j\phi}\ \mathbf{u}_1e^{j\phi}\ u_{M/2}e^{j\phi}\ \mathbf{u}_2e^{j\phi}]\triangleq[v_0\ \mathbf{v}_1\ v_{M/2}\ \mathbf{v}_2]$ (where ϕ denotes the phase offset), then $\mathbf{v}_1e^{-j\phi}=[\mathbf{v}_2e^{-j\phi}]^{\#}=e^{j\phi}\mathbf{v}_2^{\#}$ or equivalently

$$\mathbf{v}_1=e^{j2\phi}\mathbf{v}_2^{\#}. \tag{16}$$

This relation defines the CSP that is exactly possessed by the OFDM transmitted signal. Such a property can be utilized for synchronization purposes in OFDM systems with real data symbols as proposed in [17]: the end of the cyclic prefix and the phase offset can be determined by scanning the received signal and searching where such CSP is best approximated according to a least-squares approach, that is,

$$\left\{\hat{\theta}^{\mathrm{LS}},\hat{\phi}^{\mathrm{LS}}\right\}=\arg\min_{\theta,\phi}\|\mathbf{v}_1(\theta)-e^{j2\phi}\mathbf{v}_2^{\#}(\theta)\|^2 \tag{17}$$

where $\hat{\theta}$ denotes an estimate of the normalized delay $\theta_{\mathrm{id}}=\tau/T_{\mathrm{s}}$ assumed to be an integer and, moreover, the M vector $[v_0(\theta)\ \mathbf{v}_1(\theta)\ v_{M/2}(\theta)\ \mathbf{v}_2(\theta)]$ has been extracted at the candidate delay θT_{s}. Note that the maximization procedure in (17) provides a closed-form solution for the phase estimate $\hat{\phi}^{\mathrm{LS}}$ and, then, the ST estimation requires only a one-dimensional search:

$$\hat{\theta}^{\mathrm{LS}}=\arg\max_{\theta}\left\{2|\mathbf{v}_1(\theta)\cdot\mathbf{v}_2^{\#}(\theta)|-\|\mathbf{v}_1(\theta)\|^2-\|\mathbf{v}_2(\theta)\|^2\right\}. \tag{18}$$

A slightly different approach, which is aimed at simplifying the threshold setting, is often suggested (see [18] and references therein):

$$\hat{\theta}^{\mathrm{LS}}\triangleq\arg\max_{\theta}\frac{2|\mathbf{v}_1(\theta)\cdot\mathbf{v}_2^{\#}(\theta)|}{\|\mathbf{v}_1(\theta)\|^2+\|\mathbf{v}_2(\theta)\|^2}. \tag{19}$$

Note that, though not explicitly represented in the notation, the statistics in (19) depends on the length of the interval $[v_0\ \mathbf{v}_1\ v_{M/2}\ \mathbf{v}_2]$ from which the vectors $\mathbf{v}_1$ and $\mathbf{v}_2$ of length $\frac{M}{2}-1$ are extracted. In the present section a length M is considered while in the next sections a length $\frac{M}{2}$ is used.

IV. The Approximate Conjugate-Symmetry Property in OFDM/OQAM

In OFDM/OQAM systems, as noted in section II, the mth component of the vector $\mathbf{w}$ in (15) is not unit but it is equal

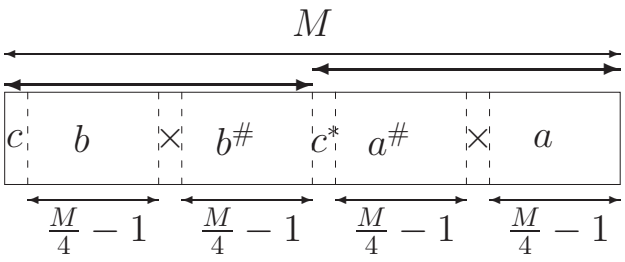

Fig. 3. The structure of each of the N_{b} equal symbols in the considered preamble for OFDM/OQAM systems when the multiplication by $\mathbf{w}$ is taken into account (left cyclic shift). The definition of the introduced symbols is explained in the caption of figure 2.

to $j^m = \exp(j2\pi\frac{1}{4}m)$, while the vectors $\mathbf{a}_n^{(\mathrm{R})}$ and $\mathbf{a}_n^{(\mathrm{I})}$ are real-valued; consequently, from (10) and (15) it follows that each vector $\mathbf{b}_n^{(\mathrm{R})}$ and $\mathbf{b}_n^{(\mathrm{I})}$ possesses a particular structure that derives from the cyclic shift of $M/4$ samples on the left. As shown in Figure 3, this implies that, for each vector of length M, two adjacent intervals of length $\frac{M}{2}$ can be singled out; in both intervals, the classical CS property reported in Figure 2 holds. Therefore we can use the same test in (19) with reference to intervals of length $\frac{M}{2}$ in order to estimate the position of such intervals if we had to operate on sequence of vectors $\{\mathbf{b}_n^{(\mathrm{R})}\}$. According to relations (2), (13), and (14), the conjugate symmetry (that is exhibited by $\mathbf{b}_n^{(\mathrm{R})}$) is destroyed by the fact that there is not any specific property capable to pass such properties from $\mathbf{b}_n^{(\mathrm{R})}$ to the transmitted signal. However, at the beginning of the burst transmission, some properties are present that are independent of the transmitted symbols and can be therefore exploited for blind synchronization. For sake of clearness, we illustrate such properties with reference to the prototype filter derived in [9] by using the frequency sampling technique and in the case where the overlap parameter is K=4. Let us first note that from (11)

$$\begin{aligned}
\mathbf{d}_{0,\mathrm{s}}^{(\mathrm{R})} &= \mathbf{g}_{0,\mathrm{s}} \times \mathbf{b}_{0,\mathrm{s}}^{(\mathrm{R})} \\
\mathbf{d}_{0,\mathrm{i}}^{(\mathrm{R})} &= \mathbf{g}_{0,\mathrm{i}} \times \mathbf{b}_{0,\mathrm{i}}^{(\mathrm{R})} \\
\mathbf{d}_{1,\mathrm{s}}^{(\mathrm{R})} &= \mathbf{g}_{0,\mathrm{s}} \times \mathbf{b}_{1,\mathrm{s}}^{(\mathrm{R})} + \mathbf{g}_{1,\mathrm{s}} \times \mathbf{b}_{0,\mathrm{s}}^{(\mathrm{R})} \\
\mathbf{d}_{1,\mathrm{i}}^{(\mathrm{R})} &= \mathbf{g}_{0,\mathrm{i}} \times \mathbf{b}_{1,\mathrm{i}}^{(\mathrm{R})} + \mathbf{g}_{1,\mathrm{i}} \times \mathbf{b}_{0,\mathrm{i}}^{(\mathrm{R})} \\
\mathbf{d}_{2,\mathrm{s}}^{(\mathrm{R})} &= \mathbf{g}_{0,\mathrm{s}} \times \mathbf{b}_{2,\mathrm{s}}^{(\mathrm{R})} + \mathbf{g}_{1,\mathrm{s}} \times \mathbf{b}_{1,\mathrm{s}}^{(\mathrm{R})} + \mathbf{g}_{2,\mathrm{s}} \times \mathbf{b}_{0,\mathrm{s}}^{(\mathrm{R})}
\end{aligned} \tag{20}$$

where we denote with $\mathbf{d}_{k,\mathrm{s}}^{(\mathrm{R})}$, $\mathbf{g}_{k,\mathrm{s}}$, and $\mathbf{b}_{k,\mathrm{s}}^{(\mathrm{R})}$ (for $k = 0, 1, 2$) the vectors obtained from $\mathbf{d}_k^{(\mathrm{R})}$, $\mathbf{g}_k$, and $\mathbf{b}_k^{(\mathrm{R})}$, respectively, by extracting the first $M/2$ components; moreover, we denote with $\mathbf{d}_{k,\mathrm{i}}^{(\mathrm{R})}$, $\mathbf{g}_{k,\mathrm{i}}$, and $\mathbf{b}_{k,\mathrm{i}}^{(\mathrm{R})}$ the vectors obtained from $\mathbf{d}_k^{(\mathrm{R})}$, $\mathbf{g}_k$, and $\mathbf{b}_k^{(\mathrm{R})}$, respectively, by extracting the last $M/2$ components. Analogously, relation (20) can be re-written with reference to the PPN in (14) by replacing the superscript R with I. The impulse response of the considered prototype filter is reported in Figure 4 where the intervals used to extract from the prototype filter the vectors $\mathbf{g}_{0,\mathrm{s}}$, $\mathbf{g}_{0,\mathrm{i}}$, $\mathbf{g}_{1,\mathrm{s}}$, $\mathbf{g}_{1,\mathrm{i}}$, $\mathbf{g}_{2,\mathrm{s}}$, and $\mathbf{g}_{2,\mathrm{i}}$, introduced in (20), are specified. Let us remind that the vector $\mathbf{b}_0^{(\mathrm{R})}$ exhibits the properties described by Figure 3 and, therefore, the vector $\mathbf{b}_{0,\mathrm{i}}^{(\mathrm{R})}$ exhibits the classical property described in Figure 2 over an interval of length $\frac{M}{2}$. The multiplication by $\mathbf{g}_{0,\mathrm{i}}$ in (20) implies that $\mathbf{d}_{0,\mathrm{i}}^{(\mathrm{R})}$ does not possess exactly the CS property. However, such a property is approximately present since the entries of $\mathbf{g}_{0,\mathrm{i}}$ are all negative real values. In fact, the original scalar product in (19) for two equal vectors $\mathbf{v}_1$ and $\mathbf{v}_2^{\#}$ resulting from the exact CS property in $\mathbf{b}_{0,\mathrm{i}}^{(\mathrm{R})} = [v_0\ \mathbf{v}_1\ v_{\frac{M}{4}}\ \mathbf{v}_2]$

$$|\mathbf{v}_1 \cdot \mathbf{v}_2^{\#}| = \left| \sum_{m=0}^{\frac{M}{4}-2} v_{1,m} v_{2,\frac{M}{4}-2-m} \right| = \sum_{m=0}^{\frac{M}{4}-2} |v_{1,m}(\theta)|^2 \tag{21}$$

($v_{\mathrm{i},m}$ denotes the mth component of the vector $\mathbf{v}_{\mathrm{i}}$ for $m \in \{0, 1, \ldots, \frac{M}{4} - 2\}$) becomes, when referred to $\mathbf{d}_{0,\mathrm{i}}^{(\mathrm{R})} = \mathbf{g}_{0,\mathrm{i}} \times \mathbf{b}_{0,\mathrm{i}}^{(\mathrm{R})}$,

$$\begin{aligned}
&\left| \sum_{m=0}^{\frac{M}{4}-2} \left[v_{1,m}\ g_{0,\mathrm{i},m+1} \right] \left[v_{2,\frac{M}{4}-2-m} g_{0,\mathrm{i},\frac{M}{2}-1-m} \right] \right| \\
&\qquad = \left| \sum_{m=0}^{\frac{M}{4}-2} |v_{1,m}|^2\ g_{0,\mathrm{i},m+1}\ g_{0,\mathrm{i},\frac{M}{2}-1-m} \right|
\end{aligned} \tag{22}$$

where $g_{0,\mathrm{i},m}$ denotes the mth entry of $\mathbf{g}_{0,\mathrm{i}}$ for $m \in \{0, 1, 2, \ldots, \frac{M}{2} - 1\}$. Since now $g_{0,\mathrm{i},m+1} \neq g_{0,\mathrm{i},\frac{M}{2}-1-m}$ there is not a conjugate symmetry but since $g_{0,\mathrm{i},m+1}\ g_{0,\mathrm{i},\frac{M}{2}-1-m} \geq 0$, the sum in the right-hand side of (22) is still positive and much larger than the value obtained for positions where such an approximate property does not hold. This permits the use of the test in (19) over intervals of length $\frac{M}{2}$ in order to detect the positions where the CS property holds if we had to operate over a sequence of vectors $\{\mathbf{d}_n^{(\mathrm{R})}\}$. Let us note that this approximately holds also if the sign of $g_{0,\mathrm{i},m+1} g_{0,\mathrm{i},\frac{M}{2}-1-m}$ is not constant; in fact, if such a sign assumes the same value for a large percentage of the $\frac{M}{4} - 1$ values of the sum in (22), then the term in the right-hand side of (22) is much larger than that obtained for a generic position where such an approximate property does not hold. Therefore, the approximate CS property can be detected by the test in (19) provided that a large percentage of terms in the sum in (22) has the same sign. The delay of $M/2$ samples that the output of the PPN in (14) exhibits with reference to the output of the PPN in (13) implies that

$$\begin{aligned}
\mathbf{d}_0^{(\mathrm{T})} &= \mathbf{g}_{0,\mathrm{s}} \times \mathbf{b}_{0,\mathrm{s}}^{(\mathrm{R})} \\
\mathbf{d}_1^{(\mathrm{T})} &= \mathbf{g}_{0,\mathrm{i}} \times \mathbf{b}_{0,\mathrm{i}}^{(\mathrm{R})} + \mathbf{g}_{0,\mathrm{s}} \times \mathbf{b}_{0,\mathrm{s}}^{(\mathrm{I})} \\
\mathbf{d}_2^{(\mathrm{T})} &= \mathbf{g}_{0,\mathrm{s}} \times \mathbf{b}_{1,\mathrm{s}}^{(\mathrm{R})} + \mathbf{g}_{1,\mathrm{s}} \times \mathbf{b}_{0,\mathrm{s}}^{(\mathrm{R})} + \mathbf{g}_{0,\mathrm{i}} \times \mathbf{b}_{0,\mathrm{i}}^{(\mathrm{I})} \\
\mathbf{d}_3^{(\mathrm{T})} &= \mathbf{g}_{0,\mathrm{i}} \times \mathbf{b}_{1,\mathrm{i}}^{(\mathrm{R})} + \mathbf{g}_{1,\mathrm{i}} \times \mathbf{b}_{0,\mathrm{i}}^{(\mathrm{R})} + \mathbf{g}_{0,\mathrm{s}} \times \mathbf{b}_{1,\mathrm{s}}^{(\mathrm{I})} \\
&+ \mathbf{g}_{1,\mathrm{s}} \times \mathbf{b}_{0,\mathrm{s}}^{(\mathrm{I})} \\
\mathbf{d}_4^{(\mathrm{T})} &= \mathbf{g}_{0,\mathrm{s}} \times \mathbf{b}_{2,\mathrm{s}}^{(\mathrm{R})} + \mathbf{g}_{1,\mathrm{s}} \times \mathbf{b}_{1,\mathrm{s}}^{(\mathrm{R})} + \mathbf{g}_{2,\mathrm{s}} \times \mathbf{b}_{0,\mathrm{s}}^{(\mathrm{R})} \\
&+ \mathbf{g}_{0,\mathrm{i}} \times \mathbf{b}_{1,\mathrm{i}}^{(\mathrm{I})} + \mathbf{g}_{1,\mathrm{i}} \times \mathbf{b}_{0,\mathrm{i}}^{(\mathrm{I})}
\end{aligned} \tag{23}$$

where the vector $\mathbf{d}_0^{(\mathrm{T})}$ contains the first block of $M/2$ samples of the transmitted signal while $\mathbf{d}_1^{(\mathrm{T})}$ contains the second block of $M/2$ samples of the same signal and so on. Let us take into account that the choice of the prototype filter derived in [9] implies $\|\mathbf{g}_0\| \ll \|\mathbf{g}_1\|$; moreover, $\|\mathbf{g}_{0,\mathrm{s}}\| \ll \|\mathbf{g}_{0,\mathrm{i}}\|$ and $\|\mathbf{g}_{1,\mathrm{s}}\| \ll \|\mathbf{g}_{1,\mathrm{i}}\|$. Finally, $\|\mathbf{g}_{2,\mathrm{s}}\| \gg \|\mathbf{g}_{2,\mathrm{i}}\|$ and $\|\mathbf{g}_{2,\mathrm{s}}\| =$

$\|\mathbf{g}_{1,\mathrm{i}}\|$. Consequently, (23) can be approximated as

$$\begin{array}{lcl} \mathbf{d}_0^{(\mathrm{T})} & = & \mathbf{g}_{0,\mathrm{s}} \times \mathbf{b}_{0,\mathrm{s}}^{(\mathrm{R})} \\ \mathbf{d}_1^{(\mathrm{T})} & \simeq & \mathbf{g}_{0,\mathrm{i}} \times \mathbf{b}_{0,\mathrm{i}}^{(\mathrm{R})} \\ \mathbf{d}_2^{(\mathrm{T})} & \simeq & \mathbf{g}_{1,\mathrm{s}} \times \mathbf{b}_{0,\mathrm{s}}^{(\mathrm{R})} \\ \mathbf{d}_3^{(\mathrm{T})} & \simeq & \mathbf{g}_{1,\mathrm{i}} \times \mathbf{b}_{0,\mathrm{i}}^{(\mathrm{R})} \\ \mathbf{d}_4^{(\mathrm{T})} & \simeq & \mathbf{g}_{2,\mathrm{s}} \times \mathbf{b}_{0,\mathrm{s}}^{(\mathrm{R})} + \mathbf{g}_{1,\mathrm{i}} \times \mathbf{b}_{0,\mathrm{i}}^{(\mathrm{I})} \end{array} \tag{24}$$

The terms $\mathbf{d}_k^{(\mathrm{T})}$ for $k \geq 5$ share the structure of $\mathbf{d}_4^{(\mathrm{T})}$ since for $k \geq 5$ the two vectors with stronger entries are both present. From the previous discussion, it follows that, for $k \in \{0,1,2,3\}$, $\mathbf{d}_k^{(\mathrm{T})}$ possesses an approximate conjugate symmetry. With reference to the choice here considered, the entries of the vector $\mathbf{g}_{0,\mathrm{s}}$ are very weak so that $\mathbf{d}_0^{(\mathrm{T})}$ is usually buried in the noise but also the entries of $\mathbf{d}_1^{(\mathrm{T})}$ and $\mathbf{d}_2^{(\mathrm{T})}$ are weak since the two leading vectors are $\mathbf{g}_{2,\mathrm{s}}$ and $\mathbf{g}_{1,\mathrm{i}}$, which include a large fraction of the prototype-filter energy. The vector $\mathbf{d}_3^{(\mathrm{T})}$ is the first vector which is contributed by one of the two leading vectors so that $\mathbf{d}_3^{(\mathrm{T})}$ is the first vector whose power is not negligible at usual signal-to-noise ratios; moreover, $\mathbf{g}_{1,\mathrm{i}}$ and $\mathbf{g}_{0,\mathrm{i}}$ possess a constant sign of the folded vector while $\mathbf{g}_{1,\mathrm{s}}$ possesses a non-marginal percentage of its $M/4$ entries of the folded vector with a different sign. Therefore, we can deduce that the test for approximate CS property achieves its maximum for $\mathbf{d}_3^{(\mathrm{T})}$ while the values relative to $\mathbf{d}_1^{(\mathrm{T})}$ and $\mathbf{d}_2^{(\mathrm{T})}$ are much smaller. Finally, note that the vectors $\mathbf{d}_k^{(\mathrm{T})}$ for $k \geq 4$ are contributed both by $\mathbf{g}_{2,\mathrm{s}}$ and $\mathbf{g}_{1,\mathrm{i}}$ and, consequently, they do not exhibit significant values to the test (19). In fact, by using the approximation (24) for $\mathbf{d}_4^{(\mathrm{T})}$ in the scalar product of the test (19), we do not obtain any guarantee that the $M/4-1$ values summed up in the scalar product maintain themselves coherent. Thus, when we look for a position of conjugate symmetry in the received signal $r(i)$ (seen as a sequence of vectors $\mathbf{d}_n^{(\mathrm{T})}$) observed at the channel output by using the test (19) over intervals of length $\frac{M}{2}$

$$\Psi(\theta) \stackrel{\triangle}{=} \frac{2\left|\sum_{i=0}^{\frac{M}{4}-1} r(\theta-i)r(\theta+i)\right|}{\sum_{i=0}^{\frac{M}{4}-1}|r(\theta-i)|^2 + \sum_{i=0}^{\frac{M}{4}-1}|r(\theta+i)|^2} \tag{25}$$

we obtain the argument of the top value ($\theta = \theta_1$) of the statistics $\Psi(\theta)$ in correspondence of the interval where the vector $\mathbf{d}_3^{(\mathrm{T})}$ is present. The beginning of such an interval is shifted by $3M/2$ samples at the right of the beginning of the burst and θ_1, which denotes the central value of such an interval according to (25), is shifted of $7M/4$ samples from the first sample of the burst. Moreover, M samples on the left of the top value, we find another maximum ($\theta = \theta_3$) of the statistics due to the properties of $\mathbf{d}_1^{(\mathrm{T})}$ and, in the middle point between them, we find a second maximum ($\theta = \theta_2$) due to the properties of $\mathbf{d}_2^{(\mathrm{T})}$.

Note that, though $\|\mathbf{g}_{1,\mathrm{s}}\| \gg \|\mathbf{g}_{0,\mathrm{i}}\|$, the value of the maximum in θ_2 is only slightly larger than that in θ_3 since the signs of the components of $\mathbf{g}_{1,\mathrm{s}}$, unlike those of $\mathbf{g}_{0,\mathrm{i}}$, are not constant. There is also a fourth maximum ($\theta = \theta_4$) due to the properties of $\mathbf{d}_0^{(\mathrm{T})}$, buried in noise at usual signal-to-noise ratios. Therefore, the argument of the top value ($\theta = \theta_1$) of the statistic in (25) can be used for blindly estimating the beginning of a burst of OFDM/OQAM symbols as $\theta_1 - \frac{7M}{4}$. In Fig. 5 we report a typical realization of the statistics in (25) in AWGN for $E_b/N_o = 20$ dB and $M = 1024$. Although derived for the sake of clearness with reference to the case $K = 4$, often considered in OFDM/OQAM literature, the method can be straightforwardly extended to other values of K.

Let us finally note that the statistics $\Psi(\theta)$ in (25) is independent of the frequency offset ε; the derivation of the method B in Section V implicitly sketches the prove of this for the scalar product in the numerator of (25).

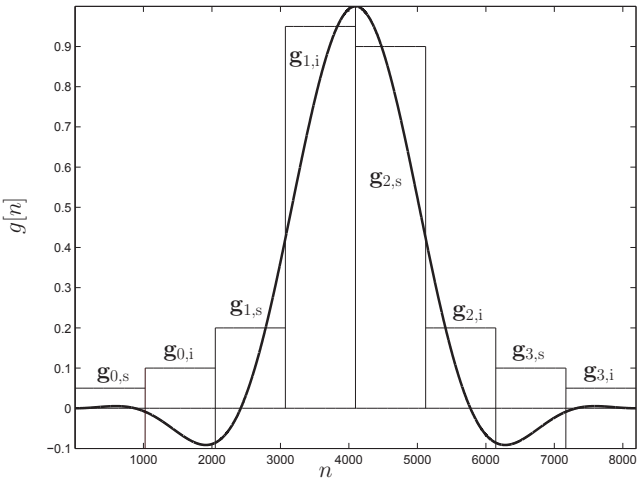

Fig. 4. The prototype filter and the vectors $\mathbf{g}_{0,\mathrm{s}}$, $\mathbf{g}_{0,\mathrm{i}}$, $\mathbf{g}_{1,\mathrm{s}}$, $\mathbf{g}_{1,\mathrm{i}}$, $\mathbf{g}_{2,\mathrm{s}}$, $\mathbf{g}_{2,\mathrm{i}}$, $\mathbf{g}_{3,\mathrm{s}}$, and $\mathbf{g}_{3,\mathrm{i}}$. The time axis refers to the choice $M = 2048$ but the same partition holds also for other values of M.

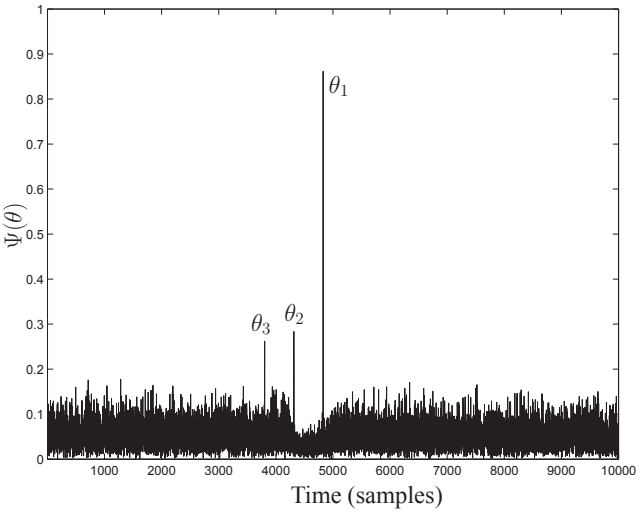

Fig. 5. A typical realization of the statistics $\Psi(\theta)$ in (25) in AWGN for $E_b/N_o = 20$ dB and $M = 1024$. We denote with θ_1, θ_2 and θ_3 the values of θ corresponding to the three maxima of $\Psi(\theta)$. In the present example, $\theta_1 = 4828$ while the burst begins at $\theta = 3036$.

V. Blind CFO Estimation

In this section we introduce two different methods for blind CFO estimation. The first method, dubbed method A, can be

derived from the fact that from (24),

$$\mathbf{D}_3^{(\mathrm{T})} \triangleq \frac{\mathbf{d}_3^{(\mathrm{T})}}{\mathbf{g}_{1,\mathrm{i}}} \simeq \frac{\mathbf{d}_1^{(\mathrm{T})}}{\mathbf{g}_{0,\mathrm{i}}} \triangleq \mathbf{D}_1^{(\mathrm{T})} \tag{26}$$

where the division between the two vectors is defined component-wise. Consequently, in the presence of a normalized frequency-offset ε and neglecting the presence of noise and the effects of the channel, the entries of the vector $\mathbf{D}_3^{(\mathrm{T})}/\mathbf{D}_1^{(\mathrm{T})}$ are all equal to $\exp(j2\pi\frac{\varepsilon}{M}M) = \exp(j2\pi\varepsilon)$ since $\mathbf{d}_1^{(\mathrm{T})}$ is extracted M samples on the left of $\mathbf{d}_3^{(\mathrm{T})}$. Therefore, we evaluate the angle $\hat{\phi}_A$ of the average of the entries of $\mathbf{D}_3^{(\mathrm{T})}/\mathbf{D}_1^{(\mathrm{T})}$ and, then, we estimate the unknown CFO as $\hat{\phi}_A/(2\pi)$. In calculating the average, we do not use the entries of $\mathbf{D}_3^{(\mathrm{T})}/\mathbf{D}_1^{(\mathrm{T})}$ with amplitude larger than 2 as they are assumed to be outliers. Note that the extraction of the vectors $\mathbf{d}_k^{(\mathrm{T})}$ requires a previous ST estimation and that the errors in timing compensation worsen the performance of the CFO estimator.

The method B uses the property that, under ideal condition, the angles in the scalar products corresponding to the top value ($\theta = \theta_1$) of the statistics in (25) and the value in $\theta = \theta_2$, which is $M/2$ samples at its left, differ only due to the presence of the CFO. More specifically, such a difference is equal to $2\pi\varepsilon + \pi$ and the condition is ideal since it neglects the mismatch in the timing synchronization (obtained at the previous step), the effects of the channel and the presence of noise. Under such ideal conditions, the scalar product in (25) at $\theta = \theta_2$ can be written as follows:

$$\mathbf{v}_1^{(\varepsilon,g)}(\theta_2) \cdot \mathbf{v}_2^{(\varepsilon,g)\#}(\theta_2) = \sum_{m=0}^{\frac{M}{4}-2} v_{1,m}^{(\varepsilon,g)}(\theta_2) v_{2,\frac{M}{4}-2-m}^{(\varepsilon,g)}(\theta_2) \tag{27}$$

with the mth component $v_{\mathrm{l},m}^{(\varepsilon,g)}(\theta_2)$ of the vector $\mathbf{v}_{\mathrm{l}}^{(\varepsilon,g)}(\theta_2)$ ($m \in \{0,1,\ldots,\frac{M}{4}-2\}$ and $\mathrm{l} \in \{1,2\}$) defined as

$$\begin{cases} v_{1,m}^{(\varepsilon,g)}(\theta_2) \triangleq v_{1,m}(\theta_2) g_{1,\mathrm{s},m+1}\ e^{j2\pi\frac{\varepsilon}{M}m}\ e^{j\phi} \\ v_{2,m}^{(\varepsilon,g)}(\theta_2) \triangleq v_{2,m}(\theta_2) g_{1,\mathrm{s},\frac{M}{4}+m+1}\ e^{j2\pi\frac{\varepsilon}{M}m}\ e^{j2\pi\frac{\varepsilon}{M}\frac{M}{4}}\ e^{j\phi} \end{cases} \tag{28}$$

for $m \in \{0,1,\ldots,\frac{M}{4}-2\}$, where $v_{\mathrm{l},m}(\theta_2)$ is the mth component of the vector $\mathbf{v}_{\mathrm{l}}(\theta_2)$ ($m \in \{0,1,\ldots,\frac{M}{4}-2\}$ and $\mathrm{l} \in \{1,2\}$), $g_{1,\mathrm{s},m}$ is the mth component of the vector $\mathbf{g}_{1,\mathrm{s}}$ (for $m \in \{0,1,\ldots,\frac{M}{2}-1\}$) and ϕ is a constant phase offset. The CS property implies that $\mathbf{v}_1(\theta_2) = \mathbf{v}_2^{\#}(\theta_2)$ (i.e., $v_{1,m}(\theta_2) = v_{2,\frac{M}{4}-2-m}^{*}(\theta_2)$ $m \in \{0,1,\ldots,\frac{M}{4}-2\}$) and, consequently, (27) becomes

$$\begin{aligned} \mathbf{v}_1^{(\varepsilon,g)}(\theta_2) \cdot \mathbf{v}_2^{(\varepsilon,g)\#}(\theta_2) &= \sum_{m=0}^{\frac{M}{4}-2} \left(v_{1,m}(\theta_2) g_{1,\mathrm{s},m+1} e^{j2\pi\frac{\varepsilon}{M}m} e^{j\phi}\right) \\ &\times \left(v_{2,\frac{M}{4}-2-m}(\theta_2) g_{1,\mathrm{s},\frac{M}{4}+(\frac{M}{4}-2-m)+1} e^{j2\pi\frac{\varepsilon}{M}(\frac{M}{4}-2-m)}\right. \\ &\times \left. e^{j2\pi\frac{\varepsilon}{M}\frac{M}{4}} e^{j\phi}\right) \\ &= \sum_{m=0}^{\frac{M}{4}-2} |v_{1,m}(\theta_2)|^2 g_{1,\mathrm{s},m+1} g_{1,\mathrm{s},\frac{M}{2}-m-1} e^{j2\pi\frac{\varepsilon}{M}(\frac{M}{4}-2)} e^{j2\pi\frac{\varepsilon}{M}\frac{M}{4}} e^{j2\pi\frac{\varepsilon}{M}\frac{M}{2}} e^{j2\phi} \\ &= e^{j2\phi}\ e^{j\pi\varepsilon} e^{-j2\pi\frac{2\varepsilon}{M}} \sum_{m=0}^{\frac{M}{4}-2} |v_{1,m}(\theta_2)|^2 g_{1,\mathrm{s},m+1} g_{1,\mathrm{s},\frac{M}{2}-m-1} \end{aligned} \tag{29}$$

Analogously, the scalar product in (25) at $\theta = \theta_1$ can be therefore written as follows:

$$\mathbf{v}_1^{(\varepsilon,g)}(\theta_1) \cdot \mathbf{v}_2^{(\varepsilon,g)\#}(\theta_1) = \sum_{m=0}^{\frac{M}{4}-2} v_{1,m}^{(\varepsilon,g)}(\theta_1) v_{2,\frac{M}{4}-2-m}^{(\varepsilon,g)}(\theta_1) \tag{30}$$

with the mth component $v_{\mathrm{l},m}^{(\varepsilon,g)}(\theta_1)$ of the vector $\mathbf{v}_{\mathrm{l}}^{(\varepsilon,g)}(\theta_1)$ ($m \in \{0,1,\ldots,\frac{M}{4}-2\}$ and $\mathrm{l} \in \{1,2\}$) defined as

$$\begin{cases} v_{1,m}^{(\varepsilon,g)}(\theta_1) \triangleq v_{1,m}(\theta_1)\ g_{1,\mathrm{i},m+1}\ e^{j2\pi\frac{\varepsilon}{M}m}\ e^{j2\pi\frac{\varepsilon}{M}\frac{M}{2}}\ e^{j\phi} \\ v_{2,m}^{(\varepsilon,g)}(\theta_1) \triangleq v_{2,m}(\theta_1)\ g_{1,\mathrm{i},\frac{M}{4}+m+1}\ e^{j2\pi\frac{\varepsilon}{M}m}\ e^{j2\pi\frac{\varepsilon}{M}\frac{M}{4}} \\ \qquad \times\ e^{j2\pi\frac{\varepsilon}{M}\frac{M}{2}}\ e^{j\phi} \end{cases} \tag{31}$$

for $m \in \{0,1,\ldots,\frac{M}{4}-2\}$, where $v_{\mathrm{l},m}(\theta_1)$ is the mth component of the vector $\mathbf{v}_{\mathrm{l}}(\theta_1)$ ($m \in \{0,1,\ldots,M/4-2\}$ and $\mathrm{l} \in \{1,2\}$) and $g_{1,\mathrm{i},m}$ is the mth component of the vector $\mathbf{g}_{1,\mathrm{i}}$ (for $m \in \{0,1,2,\ldots,M/2-1\}$). The CS property implies that $\mathbf{v}_1(\theta_1) = \mathbf{v}_2^{\#}(\theta_1)$ (i.e., $v_{1,m}(\theta_1) = v_{2,\frac{M}{4}-2-m}^{*}(\theta_1)$ $m \in \{0,1,\ldots,\frac{M}{4}-1\}$) and, consequently, (30) becomes

$$\begin{aligned} \mathbf{v}_1^{(\varepsilon,g)}(\theta_1) \cdot \mathbf{v}_2^{(\varepsilon,g)\#}(\theta_1) &= \sum_{m=0}^{\frac{M}{4}-2} \left(v_{1,m}(\theta_1) g_{1,\mathrm{i},m+1} e^{j2\pi\frac{\varepsilon}{M}m}\right. \\ &\times \left. e^{j2\pi\frac{\varepsilon}{M}\frac{M}{2}} e^{j\phi}\right) \left(v_{2,\frac{M}{4}-2-m}(\theta_1) g_{1,\mathrm{i},\frac{M}{4}+(\frac{M}{4}-2-m)+1}\right. \\ &\times \left. e^{j2\pi\frac{\varepsilon}{M}(\frac{M}{4}-2-m)}\ e^{j2\pi\frac{\varepsilon}{M}\frac{M}{4}}\ e^{j2\pi\frac{\varepsilon}{M}\frac{M}{2}} e^{j\phi}\right) \\ &= \sum_{m=0}^{\frac{M}{4}-2} |v_{1,m}(\theta_1)|^2 g_{1,\mathrm{i},m+1} g_{1,\mathrm{i},\frac{M}{2}-m-1}\ e^{j2\pi\frac{\varepsilon}{M}(\frac{M}{4}-2)} \\ &\times e^{j2\pi\frac{\varepsilon}{M}\frac{M}{4}}\ e^{j2\pi\frac{\varepsilon}{M}\frac{M}{2}} 2 e^{j2\phi} = e^{j2\pi\varepsilon}\ e^{j2\phi}\ e^{j\pi\varepsilon} e^{-j2\pi\frac{2\varepsilon}{M}} \\ &\times \sum_{m=0}^{\frac{M}{4}-2} |v_{1,m}(\theta_1)|^2 g_{1,\mathrm{i},m+1} g_{1,\mathrm{i},\frac{M}{2}-m-1}. \end{aligned} \tag{32}$$

In order to evaluate the phase difference between the quantities in (29) and (32), we have to note that (see also Figure 4)

$$\sum_{m=0}^{\frac{M}{4}-2} g_{1,\mathrm{s},m+1} g_{1,\mathrm{s},\frac{M}{2}-m-1} < 0 \tag{33}$$

$$\sum_{m=0}^{\frac{M}{4}-2} g_{1,\mathrm{i},m+1} g_{1,\mathrm{i},\frac{M}{2}-m-1} > 0 \tag{34}$$

While (34) is obvious, (33) is verified with reference to the considered prototype. The method is straightforwardly adapted to a different prototype provided that the quantities in the left-hand side of (34) and (33) are nonnull. The limited variations with m of $|v_{1,m}(\theta_1)|^2$ and $|v_{1,m}(\theta_2)|^2$ imply that

$$\angle \sum_{m=0}^{\frac{M}{4}-2} |v_{1,m}(\theta_2)|^2 g_{1,\mathrm{s},m+1} g_{1,\mathrm{s},\frac{M}{2}-m-1} = \pi \tag{35}$$

$$\angle \sum_{m=0}^{\frac{M}{4}-2} |v_{1,m}(\theta_1)|^2 g_{1,\mathrm{i},m+1} g_{1,\mathrm{i},\frac{M}{2}-m-1} = 0 \tag{36}$$

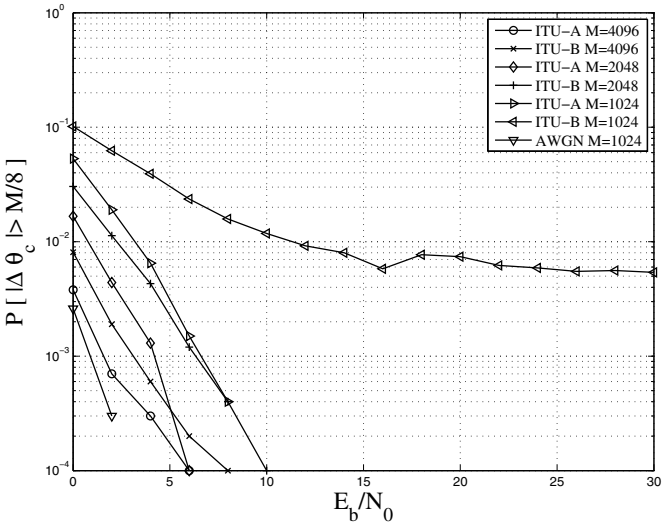

Fig. 6. Performance of the coarse estimator measured as rate for which $|\Delta\theta_c| > M/8$ where $\Delta\theta_c$ denotes the timing error of the coarse procedure.

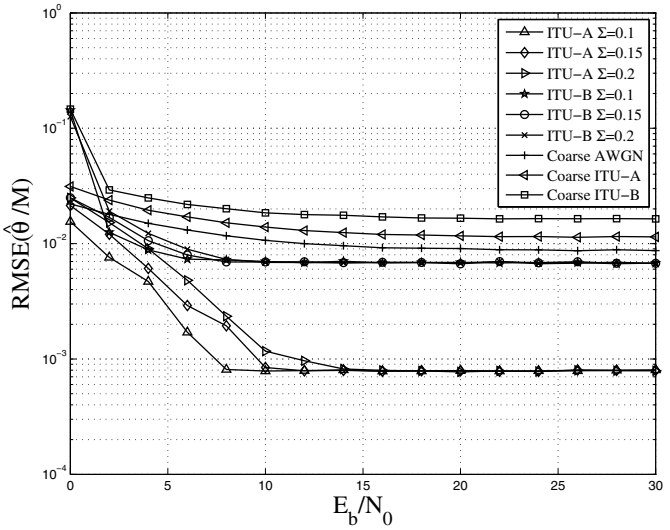

Fig. 7. RMSE of the proposed ST estimators over AWGN, ITU-A and ITU-B channels for $M = 4096$.

From (29), (32), (35), and (36) it follows that

$$\angle(\mathbf{v}_1^{(\varepsilon,g)}(\theta_1)\cdot\mathbf{v}_2^{(\varepsilon,g)\#}(\theta_1)) - \angle(\mathbf{v}_1^{(\varepsilon,g)}(\theta_2)\cdot\mathbf{v}_2^{(\varepsilon,g)\#}(\theta_2)) = 2\pi\varepsilon + \pi \tag{37}$$

Finally, we introduce the method C that defines its output as the average of the results obtained by the methods A and B. For all three methods, to avoid ambiguities in the estimate, the condition $|\varepsilon| < 0.5$ must be satisfied since they estimate ε through the complex quantity $\exp(j2\pi\varepsilon)$.

VI. Numerical Results

In this section the performance of the proposed blind methods for ST and CFO estimation is assessed via computer simulations. A number of 10^4 Monte Carlo trials has been performed under the following conditions (unless otherwise stated):

1) the considered OFDM/OQAM system has a bandwidth $B = 1/T_s = 11.2$ MHz and $M \in \{4096, 2048, 1024\}$ subcarriers while the overlap parameter K is fixed at $K = 4$;
2) all the transmitted symbols are the real and imaginary part of 4-QAM symbols;
3) the considered multipath fading channel models are the ITU Vehicular A and the ITU Vehicular B [19];
4) the channel is fixed in each run but it is independent from one run to another;
5) the timing offset is uniformly distributed in $\{3M, \ldots, 4M-1\}$, i.e., at least three symbol intervals of pure noise are included at the beginning of the transmitted signal; the overall length of the observed interval is $10M$ samples;
6) the normalized frequency offset is uniformly distributed in the range $[-0.45, 0.45]$.

Since the use of test (25) is not associated with a marginal computational complexity, we limited the use of the test to an interval of length equal to $M/4$ samples centered on the coarse estimate of the beginning of the burst. Such a coarse estimate has been obtained by filtering the squared amplitude $|r(i)|^2$ of the received signal $r(i)$ with a series of two causal moving-average filters of M samples, which are simple to implement:

$$\begin{cases} s(i) = s(i-1) + |r(i)|^2 - |r(i-M)|^2 \\ P(i) = P(i-1) + s(i) - s(i-M) \end{cases} \tag{38}$$

where we have denoted with $P(i)$ the final signal and initialized with null values the recursions $2M$ samples before the beginning of the considered interval $\{0, 1, \ldots, 10M-1\}$. Let us denote with $P_{\max}$ ($P_{\min}$) the maximum (minimum) value of $P(i)$ over the candidate interval of $10M$ samples. Then, we search the time step N_p such that

$$N_p \triangleq \arg\min_i \left| P(i) - \frac{P_{\max}+P_{\min}}{2} \right| \tag{39}$$

The coarsely estimated time-step where the burst begins is given by $N_p - \frac{11}{4}M$. In fact, according to the approximations in (24), only during the transmission of $\mathbf{d}_3^{(\mathrm{T})}$ the power of the transmitted signal is not negligible and is about the half of the power transmitted by $\mathbf{d}_k^{(\mathrm{T})}$ for $k \geq 4$. Therefore, the sequence $s(\cdot)$ will start to significantly deviate from zero $3M/2$ samples after the beginning of the burst and will roughly saturate $3M$ samples after the same beginning; consequently, the sequence $P(\cdot)$ will start to significantly deviate from zero $3M/2$ samples after the beginning of the burst and will roughly saturate $4M$ samples after the same beginning. Roughly assuming a linear increase of the sequence $P(\cdot)$ in such an interval, we obtain

$$P(i_o) \simeq \frac{P_{\max}+P_{\min}}{2} \quad \Rightarrow i_o \simeq \frac{\frac{3M}{2}+4M}{2} = \frac{11M}{4}. \tag{40}$$

The interval of $M/4$ samples for searching the properties of conjugate symmetry is then centered $\frac{7}{4}M$ samples (see Section IV for the delay between θ_1 and the beginning of the burst) after the beginning of the burst and, therefore, at time-step $N_p - M$.

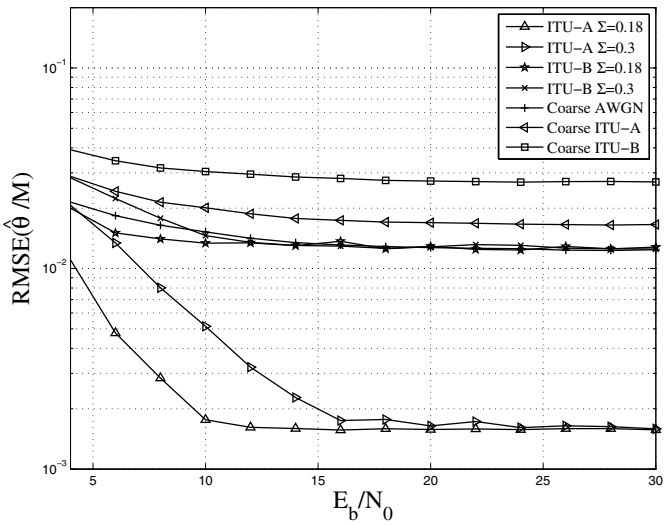

Fig. 8. RMSE of the proposed ST estimators over AWGN, ITU-A and ITU-B channels for $M = 2048$.

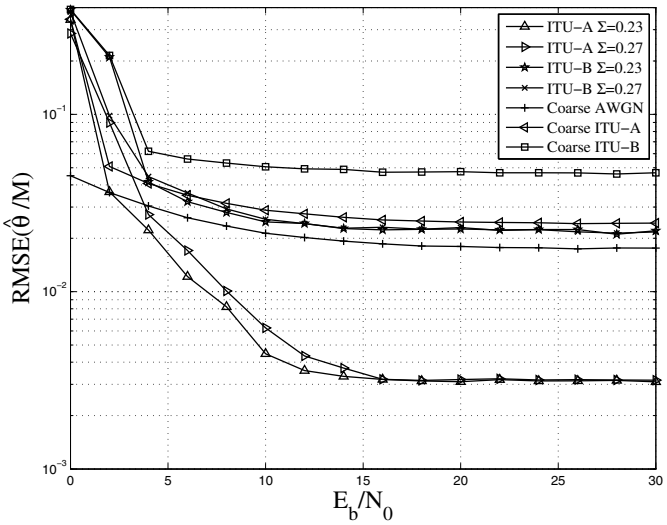

Fig. 9. RMSE of the proposed ST estimators over AWGN, ITU-A and ITU-B channels for $M = 1024$.

The noise effect on the statistics in (25) can have a significant impact since it may lead to single out a position that is not correct. In such a case, there is not guarantee that the error remains small because any time step of the observed interval may be selected. In order to reduce the effects of such outliers on the overall performance, we set a threshold Σ and we utilize the algorithm for timing estimation only when the statistics in (25) is larger than Σ; otherwise, we provide as output of the overall timing estimator the coarse estimate obtained by using (39).

Figure 6 shows the rate of wrong selection of the restricted interval by means of the coarse procedure. We notice that the coarse procedure is a valid method to restrict the search interval for larger M; however, it becomes poorer for smaller M since the interval length $M/4$ becomes smaller while the performance of the coarse procedure is practically independent of M since it filters the instantaneous power of the received signal. Note that no wrong selection has been observed on AWGN channel for $M = 2048$ and $M = 4096$.

Figure 7 displays the root mean square error (RMSE) (normalized to the number of subcarriers M) of the proposed blind ST estimator as a function of E_b/N_0 both on AWGN channel and on multipath channels ITU-A and ITU-B for $M = 4096$. It is worthwhile to emphasize that in AWGN no errors were observed in the performed 10^4 trials. For comparison purposes it is also reported the performance achieved by the coarse procedure (39) in order to appreciate the gain of the proposed method. Figure 7 shows that the smaller value of the threshold $\Sigma = 0.1$ provides improved performance over the choice $\Sigma = 0.2$. For smaller values of E_b/N_0, the choice of the threshold Σ should be optimized empirically to the system parameters: smaller values of the threshold often improve performance but also increase the probability of outliers in timing estimation. The proposed algorithm provides a strong improvement over the coarse procedure in AWGN and ITU-A channels and it allows one to achieve on ITU-B channel a performance better than that assured by the coarse procedure over AWGN channel.

Figures 8 and 9 report the same curves considered in Fig. 7 for values of $M = 2048$ and $M = 1024$, respectively. Note that for smaller values of M the performance worsen: for $M = 2048$ the performance of the proposed method on ITU-B channel is equivalent to that of the coarse method on AWGN channel while it becomes poorer for $M = 1024$. The figures provide also a reasonable interval of values of the threshold Σ that can be exploited by the estimator to achieve an acceptable performance.

Figure 10 shows that in both multipath channels $E_b/N_0 \simeq 12$ dB (in AWGN channel $E_b/N_0 \simeq 7$ dB) is needed to achieve an RMSE equal to 10%, which is determined in [20] as a tolerable input RMSE for successful frequency-domain pilot-based residual CFO compensation, while $E_b/N_0 \simeq 18$ dB is needed to achieve (except for method B) on both multipath channels an RMSE of 2%. Among the different methods here proposed, we can notice that in multipath channels and for E_b/N_0 larger than 11 dB, method A is superior to method B and they are practically equivalent otherwise; moreover, only for E_b/N_0 smaller than 14 dB, the additional complexity needed for applying method C is justified by the performance improvements. In AWGN channel, instead, method B is superior to method A for E_b/N_0 smaller than 14 dB and they are practically equivalent otherwise; consequently, the method C provides the best performance. Figures 11 and 12 show similar behaviors for different values of M with a slight increase of all the values of E_b/N_0 needed to obtain the properties just recalled. These figures show that only a limited decrease of the required value of the E_b/N_0 needed to achieve a fixed performance can be obtained by increasing the value of M.

VII. Conclusions

The problem of blind synchronization for OFDM/OQAM systems has been considered. Specifically, a new method for blind ST and CFO synchronization has been proposed by exploiting the approximate CSP of the beginning of a burst of OFDM/OQAM symbols due to the presence of the time offset. The results of the performance analysis with

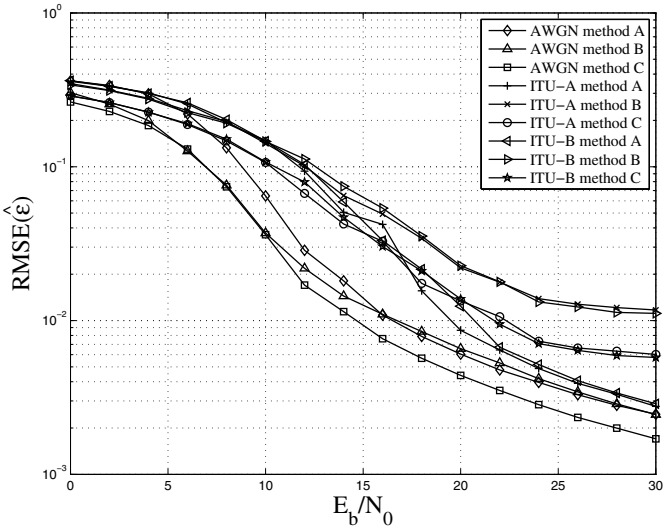

Fig. 10. RMSE of the proposed CFO estimators over AWGN, ITU-A and ITU-B channels for $M = 4096$.

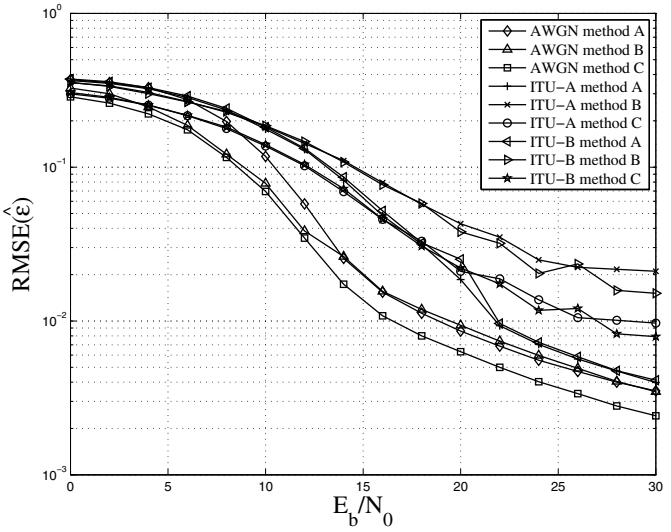

Fig. 11. RMSE of the proposed CFO estimators over AWGN, ITU-A and ITU-B channels for $M = 2048$.

reference to the considered OFDM/OQAM system show that the proposed blind ST and CFO estimators, complemented by a simpler coarse ST estimator, achieve acceptable performance for realistic values of E_b/N_0.

REFERENCES

[1] G. Cherubini, E. Eleftheriou, S. Oker, and J. Cioffi, "Filter bank modulation techniques for very high speed digital subscriber lines," *IEEE Commun. Mag.*, vol. 38, pp. 98–104, May 2000.

[2] V. Lottici, R. Reggiannini, and M. Carta, "Pilot-aided carrier frequency estimation for filter-bank multicarrier wireless communications on doubly-selective channels," *IEEE Trans. Signal Process.*, vol. 58, pp. 2783–2794, May 2010.

[3] B. Saltzberg, "Performance of an efficient parallel data transmission system," *IEEE Trans. Commun. Technol.*, vol. 15, pp. 805–811, June 1967.

[4] B. Le Floch, M. Alard, and C. Berrou, "Coded orthogonal frequency division multiplex," *Proc. IEEE*, vol. 83, pp. 982–996, June 1995.

[5] Y. Medjahdi, M. Terre, D. L. Ruyet, D. Roviras, and A. Dziri, "Performance analysis in the downlink of asynchronous OFDM/FBMC based multi-cellular networks," *IEEE Trans. Wireless Commun.*, vol. 10, pp. 2630–2639, Aug. 2011.

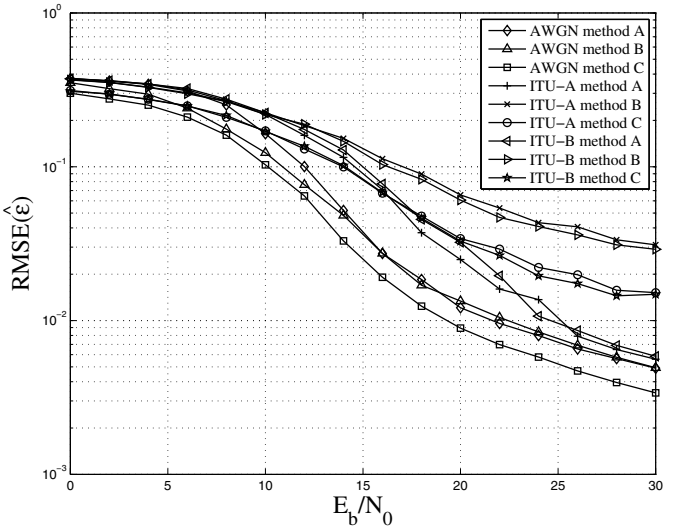

Fig. 12. RMSE of the proposed CFO estimators over AWGN, ITU-A and ITU-B channels for $M = 1024$.

[6] R. Zakaria and D. L. Ruyet, "A novel filter-bank multicarrier scheme to mitigate the intrinsic interference: application to MIMO systems," *IEEE Trans. Wireless Commun.*, vol. 11, pp. 1112–1123, Mar. 2012.

[7] P. P. Vaidyanathan, *Multirate Systems and Filter Banks*. Prentice Hall, 1993.

[8] P. Siohan, C. Siclet, and N. Lacaille, "Analysis and design of OFDM/OQAM systems based on filterbank theory," *IEEE Trans. Signal Process.*, vol. 50, pp. 1170–1183, May 2002.

[9] M. Bellanger, "Specification and design of a prototype filter for filter bank based multicarrier transmissions," in *Proc. 2001 IEEE International Conf. Acoustics, Speech, Signal Process.*, vol. 4, pp. 2417–2420.

[10] T. Fusco, A. Petrella, and M. Tanda, "Data-aided symbol timing and CFO synchronization for filter-bank multicarrier systems," *IEEE Trans. Wireless Commun.*, vol. 8, pp. 2705–2715, May 2009.

[11] M. Bellanger, "Efficiency of filter bank multicarrier techniques in burst radio transmission," in *Proc. 2010 IEEE Global Commun. Conf.*, pp. 1–4.

[12] P. Ciblat and E. Serpedin, "A fine blind frequency offset estimator for OFDM/OQAM systems," *IEEE Trans. Signal Process.*, vol. 52, pp. 291–296, Jan. 2004.

[13] H. Bölcskei, "Blind estimation of symbol timing and carrier frequency offset in wireless OFDM systems," *IEEE Trans. Commun.*, vol. 49, pp. 988–999, June 2001.

[14] T. Fusco and M. Tanda, "Blind frequency-offset estimation for OFDM/OQAM systems," *IEEE Trans. Signal Process.*, vol. 55, pp. 1828–1838, May 2007.

[15] T. Fusco, A. Petrella, and M. Tanda, "Non-data-aided carrier frequency offset estimation for pulse-shaping OFDM/OQAM systems," *Signal Process.*, vol. 88, pp. 1958–1970, Aug. 2008.

[16] D. Mattera and M. Tanda, "A new method for blind synchronization for OFDM/OQAM systems," in *Proc. 2011 International Symp. Image Signal Process. Analysis*.

[17] M. Tanda, "Blind symbol-timing and frequency-offset estimation in OFDM systems with real data symbols," *IEEE Trans. Commun.*, vol. 52, pp. 1609–1612, Oct. 2004.

[18] J. Zhang and X. Huang, "Autocorrelation based coarse timing with differential normalization," *IEEE Trans. Wireless Commun.*, vol. 11, pp. 526–530, Feb. 2012.

[19] Recommendation ITU-R M. 1225: Guidelines for evaluation of radio transmission technologies for IMT-2000, 1997.

[20] T. H. Stitz, T. Ihalainen, A. Viholainen, and M. Renfors, "Pilot-based synchronization and equalization in filter bank multicarrier communications," *EURASIP J. Applied Signal Process.*, vol. 2010, 2010. Article ID 741429.

Davide Mattera was born in Ischia, Italy, on January 26, 1969. He received the Dr.Eng. degree summa cum laude in electronic engineering in 1994 and the Ph.D. degree in computer science and electronic engineering in 1998, both from the University of Napoli Federico II. Since 1998 he has been, first as Appointed Professor, successively as Assistant Professor, and now as Associate Professor of Telecommunications at the University of Napoli Federico II. His research interests include statistical signal processing, digital communications, system identification, and nonlinear signal processing.

Mario Tanda was born in Aversa, Italy, on July 15, 1963. He received the Dr. Eng. degree (summa cum laude) in electronic engineering in 1987 and the Ph.D. degree in electronic and computer engineering in 1992, both from the University of Napoli Federico II. Since 1995, he has been an Appointed Professor of Signal Theory at the University of Napoli Federico II. Moreover, he has been an Appointed Professor of Electrical Communications (from 1996 until 1997) and Telecommunication Systems (from 1997 until 2008) at the Second University of Napoli. He is currently a Full Professor of Telecommunications at the University of Napoli Federico II. His research activity is in the area of signal detection and estimation, multicarrier, and multiple access communication systems.